ATMOSPHERE-GROUND COUPLING IN THE EASTERN UNITED STATES THROUGH THE TRANSPORTABLE ARRAY

By

MATTHEW ELVIN FARRELL

A THESIS PRESENTED TO THE GRADUATE SCHOOL
OF THE UNIVERSITY OF FLORIDA IN PARTIAL FULFILLMENT
OF THE REQUIREMENTS FOR THE DEGREE OF
MASTER OF SCIENCE

UNIVERSITY OF FLORIDA

2016

ACKNOWLEDGMENTS

I thank Dr. Mark Panning for many things: for always having time for questions; for his insight with the science; for his patience from the beginning; and most especially for his support allowing me to complete at the end of my time here. I also thank Drs. Pete Adams and Liz Screaton for their careful thought and kind criticisms all along the way. I thank Dr. Ray Russo for getting me started on the path I'm on. Lastly, I thank my family: my mother, for constant love and support; my brothers, for ensuring my head never gets too big; and my grandparents, for inspiration and hope.

TABLE OF CONTENTS

LIST OF FIGURES

Figure page

LIST OF ABBREVIATIONS

LDO	1 Hz channel recording barometric pressure signal
LDF	1 Hz channel recording infrasound signal
LDt	1 Hz calculated time derivative of LDO
LHE	1 Hz channel recording east-west seismic movement
LHN	1 Hz channel recording north-south seismic movement
LHZ	1 Hz channel recording vertical seismic movement
STA/LTA	Ratio of short term average to long term average
TA	Transportable Array

Abstract of Thesis Presented to the Graduate School
of the University of Florida in Partial Fulfillment of the
Requirements for the Degree of Master of Science

ATMOSPHERE-GROUND COUPLING IN THE EASTERN UNITED STATES THROUGH THE TRANSPORTABLE ARRAY

By

Matthew Elvin Farrell

August 2016

Chair: Mark Panning
Major: Geology

It has been shown that energy can transfer into the solid-earth through differential pressure loading, atmospheric disturbances, and wind. We investigate the efficacy of this coupling through the analysis of one year of data from 419 seismic stations in the Transportable Array (TA) with collocated meteorologic sensors and suggest topography as the coupling mechanism. We show high coherence at long periods (> 100s) between horizontal seismic channels and the following atmospheric signals: barometric pressure, the time derivative of barometric pressure, and infrasound. Additionally we find low to no coherence with vertical seismic channels or at high frequencies. By overlaying signal coherence and topography we show mostly time-independent high coherence stations clustered throughout the Appalachians with few significant high coherence stations at lower elevations. For shallow seismometer installations these atmogenic signals potentially increase noise and obscure seismic information. Understanding coupling efficacy and mechanisms has potential applications in normal mode detection and planetary seismology through remote sensing.

CHAPTER 1
INTRODUCTION

Atmosphere-Ground Coupling

For the purposes of this paper, atmosphere-ground coupling represents the idea that energy can be transferred from the atmosphere into the ground – and vice versa – in the form of pressure waves. We study this phenomena from a seismological perspective and since any atmogenic signal transferred into the ground is by definition not sourced by an earthquake or other seismic event it is generally thought of as noise in a seismic signal.

A seismic signal is the convolution of multiple information signals combined with system noise. We can represent a seismic signal as

$$u(t) = x(t) * e(t) * q(t) * i(t) + N(t) \quad (1\text{-}1)$$

Here $u(t)$ represents the measured ground motion which is equal to the convolution of $x(t)$, the source time function of the earthquake (or other seismic event), $e(t)$, the elastic effects of Earth's structure on the signal, $q(t)$, the anelastic effects of Earth's structure, and $i(t)$, the instrument response – i.e. the seismometer dependent systematic distortion of the real Earth signal done by the measuring instrument, summed with $N(t)$, which represents the noise in the signal – i.e. the part of the measured signal that is not explained by the preceding functions.

If atmogenic signals are detected in a seismic signal, then at some point the energy had to transfer into the ground through some solid-earth coupling mechanism (excepting the special cases where there is direct sensor coupling as discussed below). One of the most significant coupling mechanisms is the ocean as storm winds create ocean waves that then pass energy into the solid Earth (Bromirski

and Duennebier, 2002). Seismic signals associated with ocean waves are dubbed microseisms and there are two kinds: primary and secondary microseisms – the latter of which has a higher peak frequency and amplitude. In addition to atmogenic energy propagating through the ocean into the ground, signal can be generated through direct atmosphere-ground coupling. This coupling can act through local pressure variations caused by slow moving air masses, or the buffeting of higher velocity winds.

Longuet-Higgins (1950) first described the mechanism behind secondary microseisms – the strongest peak in a typical noise spectrum. When two waves of similar frequencies propagate in opposing directions through the ocean, they create pressure variations that do not attenuate with depth. These pressure variations then displace the sea floor and result in a seismic signal – secondary microseisms. Longuet-Higgins (1950) also suggested that these opposing waves would only likely occur near the shore where wave reflections could create interference, or in cyclonic depressions (i.e. storm centers) where opposing waves could be simultaneously generated. However, almost all secondary microseism energy comes from the latter case due to a resonance between the ocean bottom and free surface that can only build in deeper waters (Longuet-Higgins, 1950). This theory has since been supported using array analysis techniques that identify the main source of secondary microseisms as ocean storms in the northern Pacific during northern winters, and similarly in southern oceans during southern winters (Rhie and Romanowicz, 2004; Stehly et al., 2006). It is therefore unsurprising that microseismic amplitudes are higher during the winter, thus revealing a seasonal variability in one of the more significant portions of a signal's noise (Peterson, 1993; Rhie and Romanowicz, 2004).

Primary microseisms are caused by the direct interactions between the sea floor and ocean waves in shallow, near-coastal waters while creating a signal peak with a generally smaller amplitude than that of secondary microseisms (Hasselman, 1963; Cessaro, 1994). As primary microseisms are sourced by waves breaking onto the shore and coastal sea floor, small-scale bathymetric variability will affect the amplitude of this signal at certain sites.

Without coupling through the ocean, atmospheric variations have still been shown to generate seismic noise. Local variations in atmospheric pressure cause fluctuations in local gravity, while global atmospheric tides result in even larger fluctuations (Warburton and Goodkind, 1977; Merriam, 1992). These gravity fluctuations then manifest as ground motion in both vertical and horizontal component measurements. The vertical component effects are mostly explained by Newtonian attraction of the sensor to the moving air masses; however, a part of the effect is due to crustal deformation under a changing atmospheric load (Zurn and Widmer, 1995). The noise detected by horizontal measurements tends to be 5 – 10 times as large and is instead caused by pressure-induced tilting of the ground as an atmospheric load moves across a region (Sorrells, 1971; Peterson, 1993).

Local winds – at speeds greater than 3 – 5 m/s – have also been correlated with heightened noise (Withers et al., 1996; Cara et al,. 2003). Unlike microseisms and pressure loading, the coupling efficacy and method for wind energy remain unclear. Heghtened wind speeds are associated with high frequency noise at some sites (Withers et al., 1996), while at other sites low frequency noise is generated (De Angelis and Bodin, 2012). In Washington state, a near-coastal site saw long period noise

dominated by wind signal and well-correlated with wind speed when winds were active (De Angelis and Bodin, 2012). Near-coastal sites in Iberia however, found that long period noise could not be explained by individual wind profiles, but rather correlated with wave swell height (Diaz et al., 2010). McNamara and Buland (2004) note that wind turbulence transfers its energy into ground motion by interacting with vegetation, buildings, and topography. This suggests that any expected wind noise signal would be dependent on the physical properties (i.e. size and rigidity) of the objects that the wind couples with and therefore wind noise can be expected to vary greatly with both the properties of the wind (speed and direction) as well as a site's local environment.

Seismic Noise Spectra

Knowing the source of a signal's noise is only a small part of understanding it. Every seismic record contains a variable amount of signal noise which obfuscates weaker components of the signal, potentially causing a loss of meaningful information. Therefore, in order to maximize a seismic signal's ($u(t)$) significance to real Earth structure and dynamics, it is useful to understand and minimize the signal's noise ($N(t)$). In order to do this, we need to look at the spectra of seismic noise.

As shown in Equation 1-1, a seismogram is presented in the time domain; however, for many types of signal processing it is more useful to view a signal in the frequency domain. Transforming the data in this way shows which frequency bands have the most power and can elucidate source, structure, and propagation properties with the right analysis.

In general, seismic noise sources affect specific frequency bands which we will generalize as either short period noise (< 1 sec), or long period noise (> 20 second). Figure 1-1 shows expected noise ranges a seismometer might record across

at various frequencies. The majority of seismic noise in the short period band comes from either wind or cultural sources. Cultural sources refer to anything man-made – especially cars and machinery. In populated areas these noise sources dominate at greater than 1 – 10 Hz (< 1 – 0.1 sec) and are often identifiable by clear diurnal patterns (Peterson, 1993; McNamara and Buland, 2004). In more remote areas short period noise from 1 – 60 HZ (1 – 0.017 sec) has been correlated with wind speed (Withers et al., 1996).

Long period seismic noise can come from a wider variety of sources. While common knowledge lists wind as a short period noise source – because it is a rapidly changing, locally experienced phenomena – one study found seismic signal from 0.033 - 0.001 Hz (30 – 1000 sec) was well-correlated with wind speed at a particular site (De Angelis and Bodin, 2012). Local atmospheric pressure changes and pressure-induced ground tilting have been linked to seismic noise from 0.002 – 0.0003 Hz (500 – 3333 sec) in the vertical component of seismic signals and at frequencies less than 0.03 Hz (> 33 sec) in the horizontal components (Sorrells, 1971; Beauduin et al., 1996). Varying atmospheric pressure can also create seismic noise at frequencies less than 0.0003 Hz (> 3333 sec) through Newtonian attraction between a seismometer's sensor and an overlying airmass (Zurn and Widmer, 1995). Beyond typical atmospheric factors (i.e. wind and pressure), certain seismometers – those with a horizontal magnetic sensitivity greater than 0.2 m/s2T or a vertical magnetic sensitivity greater than 0.5 m/s2T – can record noise between 0.003 and 0.0003 Hz (333 – 3333 sec) due to perturbations in the ambient magnetic field (Forbriger et al. 2010). The last major source of long period energy often found in seismic signals exists at the Earth's

normal modes and represents the Earth's background 'hum'. This 'hum' is different from previously mentioned noise sources in that it has a very specific power spectra with many narrow peaks at frequencies less than 0.01 Hz (> 100 sec) (e.g. Kobayashi & Nishida, 1998; Suda et al., 1998; Rhie & Romanowicz, 2004; Ardhuin et al., 2015). These modes are excited globally by large magnitude seismic events, infragravity waves in the ocean (Rhie & Romanowicz, 2004), and possibly atmospheric pressure variations (Tanimoto & Um, 1999). The specific frequencies of the amplitude peaks are dependent on the Earth's structural properties.

In between the long and short period bands lies the microseismic band. Microseisms generally represent the most significant noise feature on most seismograms and excite frequencies from 1 – 0.05 Hz (1 – 20 sec): primary microseisms peaking between 0.1 and 0.0625 Hz (10 – 16 sec) and secondary microseisms peaking between 0.25 and 0.125 (4 – 8 sec) (Rodgers et al., 1987; Peterson, 1993; McNamara and Buland, 2004). The amplitudes of the peaks of microseimic signals tend to decrease slightly during the summer months, while the central frequencies of those peaks increase slightly (Rodgers et al., 1987; Peterson, 1993; McNamara and Buland, 2004).

Data

Any attempt to study atmosphere-ground coupling from a seismic perspective necessarily will require both meteorologic and seismic data. While the United States historically has had a wealth of both kinds of data it is often spatially and temporally separated. In 2007, as part of a broader geophysics initiative dubbed EarthScope, 400 seismic stations began systematically moving across the United States with a 70 km grid spacing from west to east. These stations made up the Transportable Array (TA),

which would record data for two years at a site before moving eastward aiming to eventually provide full staged coverage across the entire US as shown in Figure 1-2.

In mid-2010, around the time the TA network was getting east of Kentucky, the seismic stations began to include pressure and infrasound sensors at every newly installed site. As a result of that decision, we now have collocated, simultaneously recorded meteorologic and seismic data with which to study atmosphere-ground coupling for the eastern United States.

We used data from three different sensors: barometric pressure data was measured by a Setra 278 pressure transducer; infrasound data was measured by a NCPA model IFS-4532 microphone; and seismic data was measured by high quality, three-component, broadband seismometers such as the Nanometrics Trillium 240 and the Streckeisen STS-2. Each sensor measured signals at both 1 and 40 HZ, with most sites continuously recorded and telemetering data for periods of two years. We pulled from TA data taken over a one year period (October 2013 through September 2014) from over 400 seismic stations. From each station we used five different channels in our analyses: LHE, LHN, LHZ, LDO, and LDF. The first 'L' in a channel name indicates a 1 Hz sampling rate. The second letter indicates the signal type: 'H' for seismic data, 'D' for data related to pressure. The third letter specifies the signal: 'E', 'N', and 'Z' refer to the east-west, north-south, and vertical components of the seismic data; 'O' refers to the barometric pressure outside the seismometer; and a channel name with a third letter 'F' records infrasound measurements.

Methodology

The bulk of our analysis is dependent on coherence calculations. The coherence between two signals is a measure of how well the information in one signal can explain

the other. The coherence function is valued between zero and one and dependent on frequency. A coherence value of zero means the information content of one signal is completely unrelated to the second signal at a particular frequency; however, if the coherence function is valued at one across every frequency, then the two signals completely explain each other's variations. The coherence for every combination of meteorologic and seismic channel was calculated by the equation below for various lengths of data records.

$$\gamma(\omega) = \frac{|E[S^*(\omega)\cdot N(\omega)]|^2}{E|S(\omega)|^2 \cdot E|N(\omega)|^2} \text{ (Beauduin et al., 1996)} \quad (1\text{-}2)$$

Where $\gamma^2(\omega)$ is the coherence (sometimes referred to as magnitude-squared coherence), $S(\omega)$ is the seismic signal (i.e. LHE, LHN, or LHZ), $N(\omega)$ is the meteorologic signal inputting noise into the seismic signal (i.e. LDO or LDF), E and is the ensemble average. Refer to Figure 1-3 for a sample plot of coherence, also called a coherogram, and instruction as to how a coherogram can be interpreted.

Prior to calculating the coherence for a set of signals, some preprocessing had to occur. As the signals we use measure stochastic processes, an ensemble average is calculated to approximate the mean background behavior of the signal. In order to calculate this, it is necessary to slice both the seismic and meteorologic records into multiple slices. We experimented with multiple time lengths for the slices from 2 to 24 hours; however, most of our analyses use 6 hour slices to calculate the ensemble average.

After slicing it was necessary to remove all slices that had gaps where either the meteorologic or seismic sensor failed to record data. We then removed data

from any time slice found to contain a seismic event using a simple STA/LTA method as an attempt to better approximate mean background behavior.

STA/LTA methods examine the ratio of the short term average over the long term average for a time series (e.g. Withers et al., 1998; Allen, 1978). These methods work for seismic event identification because generally at a particular site the background ground motion is much less energetic than when high energy seismic wave fronts pass through the site from an earthquake or similar event. STA/LTA works well when your short term window is closely matched in length to the expected length of any high energy signal you are trying to detect and your long term window is large enough to closely approximate the background mean even when an event is in the window; for well-chosen window lengths, a short term window without an event should return a STA/LTA ratio close to 1 and a short term window capturing an event would return higher ratio whose magnitude is dependent on the energy of the captured event.

When inputting slices for the ensemble average calculations, if a 'high' STA/LTA ratio was found at any time in any slice of a seismic signal (LHE, LHN, or LHZ), then the associated time slice was thrown out as it was not expected to accurately approximate the mean background behavior of a site. For determining STA/LTA ratios we used a 5 minute short window length, a 15 minute long window length, and 2.4 as a threshold for 'high' ratios. Raising the threshold allows more data slices to be included in the calculations but increases the risk of including larger events, lowering the threshold too much returns false positives caused by standard noise fluctuations and leaves few windows for analyses. After some exploration, a threshold of 2.4 was determined to be high enough to prevent false positives from removing the

majority of our data while still low enough to detect events in our chosen window lengths. Figure 1-4 illustrates how these steps are used to get coherence measurements from a month of raw data.

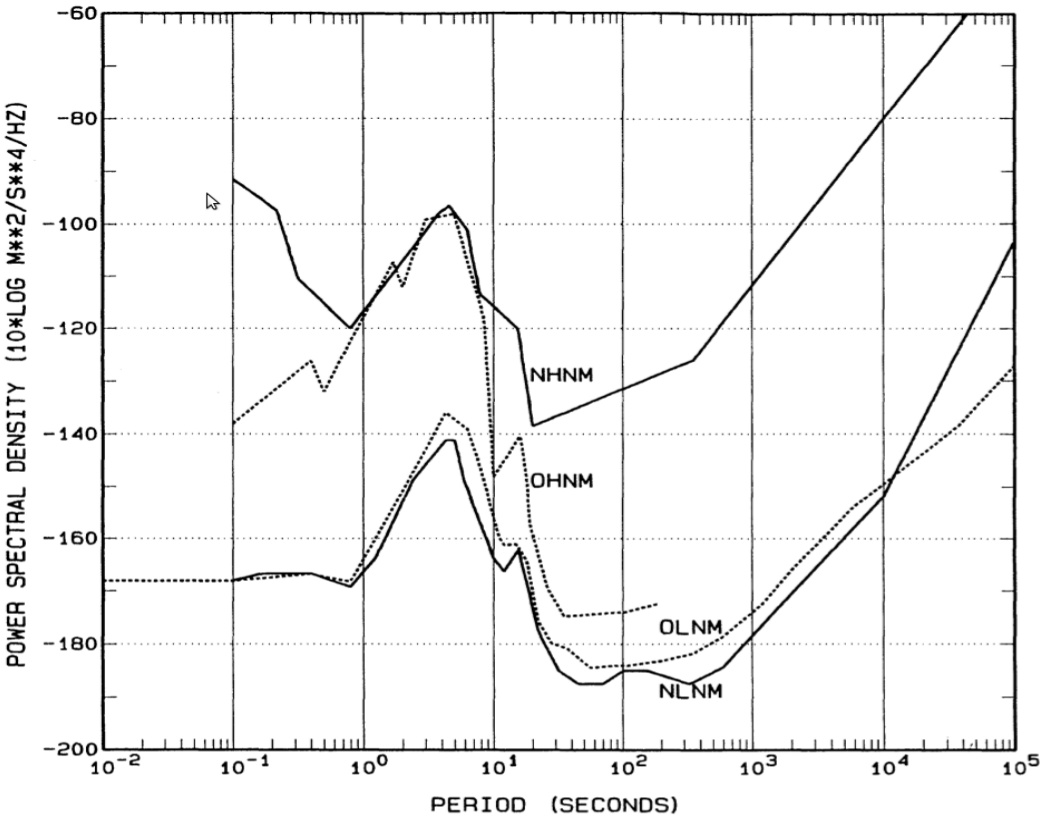

Figure 1-1. New Low Noise Model (NLNM) and New High Noise Model (NHNM) that represent the global upper and lower limits of station noise. OHNM and OLNM are models based on older data (Peterson, 1993).

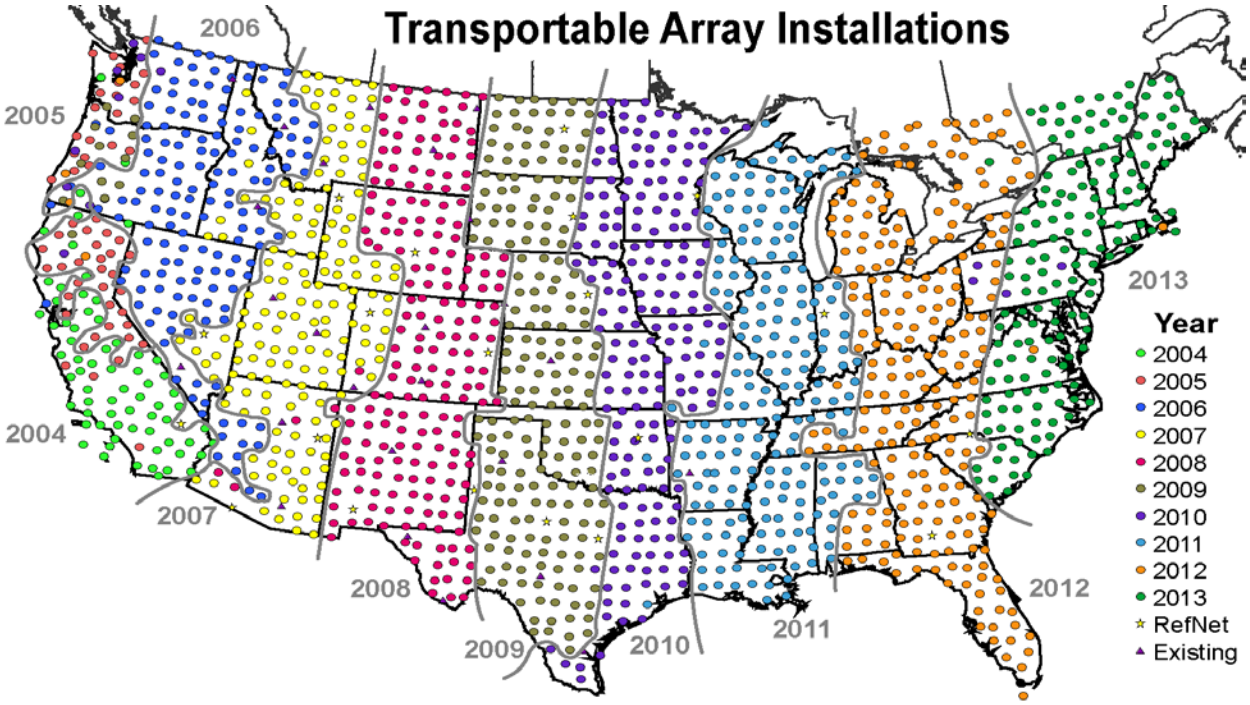

Figure 1-2. Map of the United States showing staged deployment of TA stations.

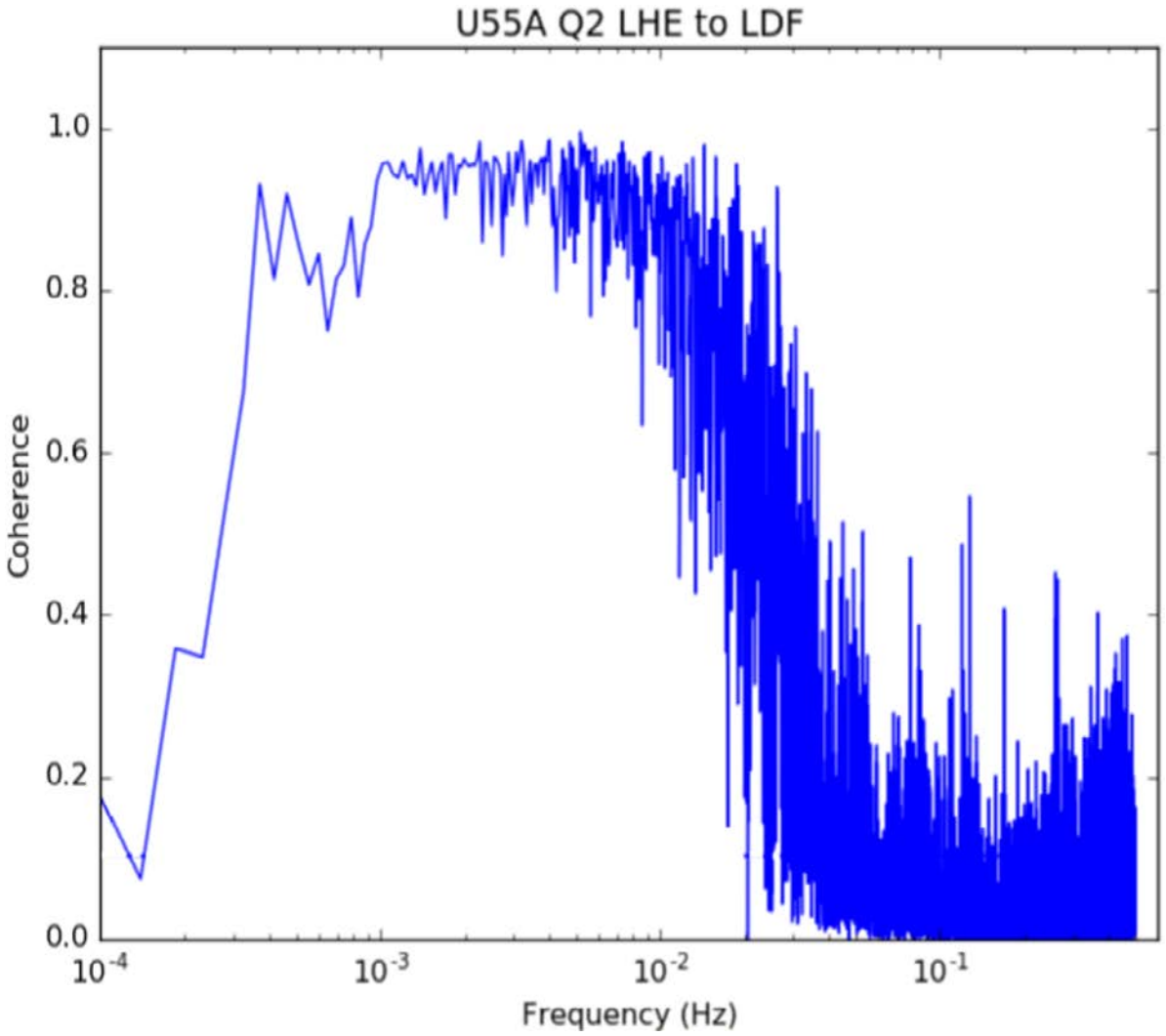

Figure 1-3. Sample coherogram. Blue line indicates the magnitude-squared coherence value between the east-west seismic signal and the infrasound signal recorded at station U55A. This coherogram indicates high long period coherence from roughly 100 – 7000 seconds and low short period coherence. A coherogram like this implies that the high frequency content of the two signals is unrelated, while showing there is a connection between the signals' low frequency content.

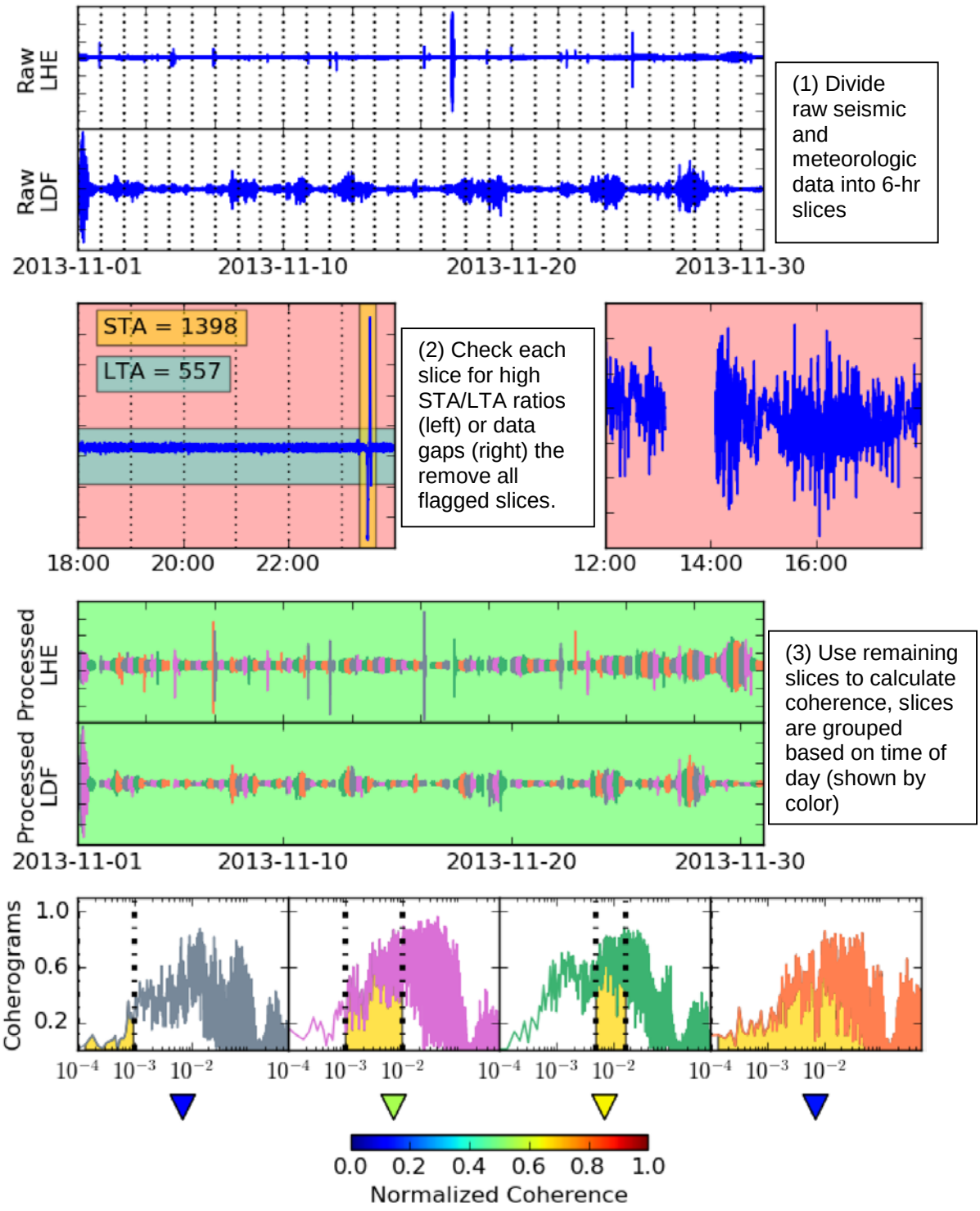

Figure 1-4. Summary of methodology for November 2013 at U55A. Note: For illustrative purposes Figure 1-4 uses window lengths of .25 and 6 hours for the STA/LTA calculations; 5 and 15 min lengths were used in actual analyses.

CHAPTER 2
RESULTS AND ANALYSIS

Assuming signals in the atmosphere and ground are not generally produced by the same source, then coherence between meteorologic and seismic signals should serve as an analogue for the efficacy of any atmosphere-ground coupling mechanisms if this coherence is calculated over a long enough time window to represent general behavior. Starting from this premise we calculated the coherence between various combinations of seismic and meteorologic signals over month long periods, we explored a few variables in the calculations and then looked for geographic and temporal pattern in the array over the course of a year.

Monthly coherograms – frequency-dependent plots of coherence – were made for 419 stations total, over 12 months, for 4 different times of day, using 9 different combinations of meteorologic and seismic channels. These variations alone account for 181008 distinct coherograms plotted, and serves as a lower limit approximation for the total number created. As it is impractical to show ~200k separate plots, I will discuss variations in coherence calculations through examples that exemplify a pattern that shows up in the broader results. The overwhelming majority of these coherograms showed little to no coherence over a broad frequency spectrum. Despite this, a number of general patterns were observed.

Diurnal Effects

As atmospheric phenomena are heavily dependent on variations due to the Earth's rotation, we hypothesized that there may be diurnal effects on atmosphere-ground coupling. To test this we divided each record day into 6 hour quarters, thus

allowing for four coherograms to be calculated for a given month (one for each quarter of the day). Figure 2-1 shows a comparison of the coherograms for the different quarters (Q01, Q02, Q03, and Q04) for station T56A during May 2014. These coherograms are typical of a station with 'very good' coherence (i.e. high coherence over a very broad frequency band). While the coherograms for T56A are not identical for each quarter, they do largely follow the same pattern with coherence above .4 for periods greater than 90 seconds.

It should be noted that the coherograms are not all made from the same amount of data. While May's 31 days allows for 31 slices to be stacked in the ensemble average of the coherence calculation, certain slices would be thrown out due to STA/LTA considerations or data gaps. As made more evident in the STA/LTA section below, this has the potential to change the coherogram significantly.

Length of Slice

While our primary analyses are based on 6-hour quarters, we did test varying the length of the record slices. Figure 2-2 shows the effect of varied slice lengths for station U55A during November 2013. All coherograms represent the first X hours of the days (in UTC time). For example, the upper-left coherogram, which is made from 12-hour slices, contains data only from 0000 – 1200 for that month. Again we see no drastic changes amongst the general shape of the coherograms – whether it is made from 2-hour, or 12-hour slices, a station showing high broad frequency coherence maintains that pattern of high broad frequency coherence independent of slice length.

A larger effect indirectly caused by varying the slice length is data loss due to our data preprocessing. Since any slices with gaps on any channel or high STA/LTA ratios on seismic channels are removed from coherence calculations, longer slices have a

higher probability of being flagged for removal from the coherence calculations. For the example in Figure 2-2 the Q01 coherogram for the 2-hour slices has data from 28 days while the 12-hour slice coherogram has data from only 15 days.

STA/LTA

As discussed above, high STA/LTA ratios can be used to identify atypical amplitudes in a signal; high STA/LTA ratios in seismic signals can indicate earthquakes. Figure 2-3 shows a comparison of coherograms for station U55A in November 2013 calculated both with and without STA/LTA considerations. The coherograms for Q01, Q02, and Q04 show significant increases in calculated coherence when the data slices with high STA/LTA ratios were removed from the ensemble averages. The coherogram for Q03 shows little difference whether STA/LTA methods are used or not; this is unsurprising considering the Q03 data contained only 3 of 30 time slices with high STA/LTA ratios while Q01 and Q04 contained 7 of 30 and Q02 contained 13 of 30. Time windows including events yield low coherences if STA/LTA methods are not used to remove them, as would be expected when earthquake signals overprint atmogenic signals.

Infrasound and the Time Derivative of Barometric Pressure

Infrasound signals (LDF) and barometric pressure (LDO) were measured at each station; however, in addition to these two signals we were interested in the time derivative of the pressure signal, which we call LDt. Since it has been shown that moving air masses (i.e. pressure fronts) can cause seismic noise (e.g. Zurn and Widmer, 1995) we hypothesized that changes in pressure – rather than its magnitude – might have a closer relationship to seismic signals.

Figure 2-4 shows coherograms calculated for station D48A during November 2013 between the east-west seismic signal (LHE) and 3 meteorologic signals: LDO, LDt, and LDF. As hypothesized, in general, the calculated LDt signal had a higher coherence with seismic channels (LHE, LHN, and LHZ) than the LDO channel. While the raw data for LDF and LDt were not equal, unexpectedly, the coherences from the two signals are nearly identical. This shows that the two signals are close to being in a constant linear relationship, and for this reason, the coherence between any signal and either LDF or LDt will be almost identical as demonstrated by the LHE-LDF and LHE-LDt overlay also in Figure 2-4.

Low Vertical Coherence

Another major observation to come out of these single station coherograms was the vertical seismic channel (LHZ) showed low coherence across a broad frequency for all station, date, time, and meteorologic signal combinations. Figure 2-5 shows 3 coherograms each based on a different quarter, station, and meteorologic signal. Despite showing broadband high coherence between horizontal seismic signals and meteorologic signals, these 3 stations have low vertical coherence. Station T56A's coherogram does show high coherence (nearly .8) for finite periods around 10 – 60 seconds; however, the coherence averaged over that band is much lower.

Maps

As outlined in Figure 1-4, a coherogram can be summarized to some extent into a single point by calculating the normalized area underneath the curve between two finite frequencies. We did this for each station while varying the factors discussed above in order to connect patterns in coherence with local geography. The points were plotted as inverted triangles at the station locations and a surface was created by interpolating

the point data; shading was added to show topographic features. The coherence values plotted are all based on 6 hour slices and use data recorded sometime between October 2013 and November 2014. The color scale stays constant for every map allowing an easy comparison between them. While data was analyzed from 419 stations, no individual map has 419 points as station coverage varies over the year. Additionally, station points were left out of the analysis if, for a given month, they did not have data from at least 10 days after STA/LTA and gap removal.

Figure 2-6 shows both the base digital elevation map used for all created maps as well as an example coherence map. The most prominent topographic feature in the study area is the Appalachian mountain chain. The mountains trend roughly northeast-southwest with a notable bend around 37.5° N – north of which the chain trends closer to north-south and south of which the chain trends closer to east-west. On the coherence map we see that cool-colored areas represent low coherence while warmer colors show areas of higher coherence. On this first coherence map we see two features that will be persistent through many long-period coherence maps: a cluster of very high coherence stations near the Appalachian bend, and a longer band of slightly heightened coherence running parallel with the entire mountain chain.

Patterns in Frequency

Figure 2-7 shows a series of seven maps where frequency is the only varied factor. These maps show the coherence between the LHE and LDF channels. The top row of maps starts on the left with high frequency data (10-2 seconds) and broadens that band to include very low frequency data (10000-2 seconds) at the rightmost map. We see in the top four maps each containing high frequency data and each showing very low coherence for all stations. The bottom row of maps progressively narrows the

frequency band towards the very low frequencies starting on the left with data from 10000-10 s and ending on the right with data from 10000-1000s. We see coherence increasing at most stations as we focus more on the long and very long period data.

Temporal Consistency

Figure 2-8 shows twelve coherence maps where the only factor varied is time. These maps all show long period (1000-100s) coherence between the LHE and LDF channels. Maps start in October 2013 and progress by month to September 2014. Four features stand out as being relatively consistent throughout time: the cluster of high coherence near the Appalachian bend, slightly heightened coherence at many stations along the Appalachian mountains with low coherence in stations at the lower elevations on each side, a cluster of 2-3 stations with high coherence directly north-west of the Appalachian bend near the Kentucky-Ohio boundary, and 1-2 stations of high coherence near Ottawa (north of New York).

It is tempting to observe a seasonal effect with heightened coherence in the spring months of March, April, and May as each of these maps are considerably warmer in color than other months. While there may be slight seasonal effects, the majority of the color warming on the maps is due to low coherence stations at the western edge dropping out of service in these months. As they drop out of service, the edges of the interpolated surface are no longer bounded by low coherences at the map's edge and thus large areas now outside of the station array are colored to match the higher coherences found in the center of the map. The maps appear to show an overall lower coherence again after spring as the highest coherence stations at the Appalachian bend begin to drop out of service as well. Figure 2-9 shows a more targeted look at seasonal effects. By focusing on the long periods (1000-100 s) we have tracked the monthly

normalized coherence for 16 stations in the center of our study area. This figure again shows that there are no broadly consistent seasonal patterns, but the stations with the highest coherence tend to have heightened coherence in late winter and early spring.

LHN-LDF

Up until now the focus has been on the east-west component of seismic motion (LHE). This focus was not necessary, but rather chosen to limit the number of variables changing at one time. Figure 2-10 shows 4 coherence maps for LHN-LDF and we see in most ways these maps are comparable to the maps of the other horizontal component (LHE). Maps (1) and (2) show that there is a similar temporal consistency in LHN-LDF, and the four features discussed in Figure 2-8 can still be seen with only small variations. We see the high coherence cluster at the Appalachian bend is broader by a couple of stations and is less separated from the small high coherence cluster to the northwest. Additionally the maps show that there is no coherence at high frequencies but coherence does increase when you focus on longer periods.

LDO

The patterns observed in infrasound coherence are similarly observed when comparing the seismic channels to the barometric pressure data (LDO) – though to a lesser magnitude. Figure 2-11 shows that long-period (1000-100 s) coherence between either LHN or LHE and LDO is mostly focused around the Appalachian chain with a cluster of heightened coherence near the Appalachian bend and few other multi-station clusters within the data set.

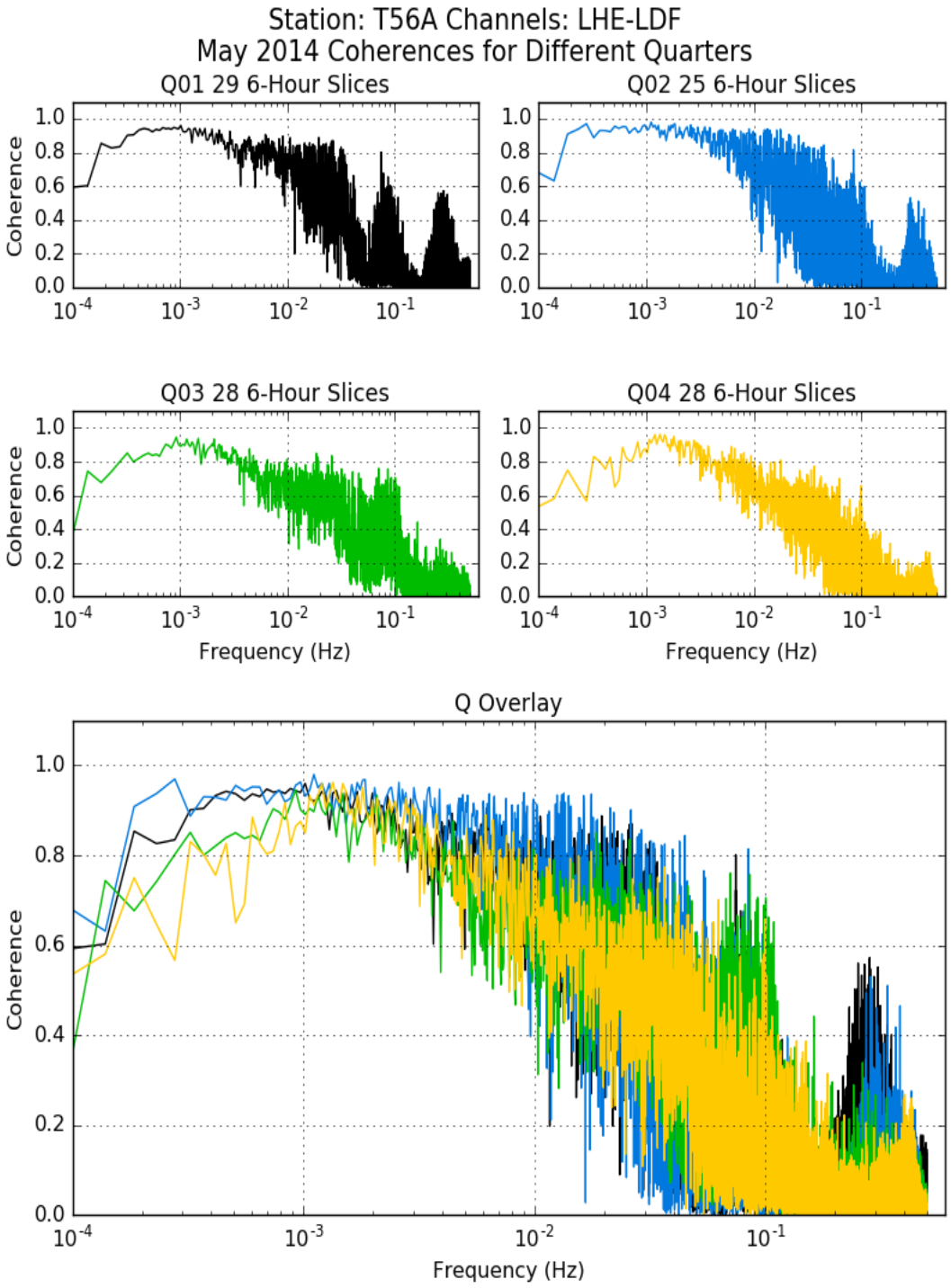

Figure 2-1. Comparison of coherograms for different times of day (Q) of recorded data.

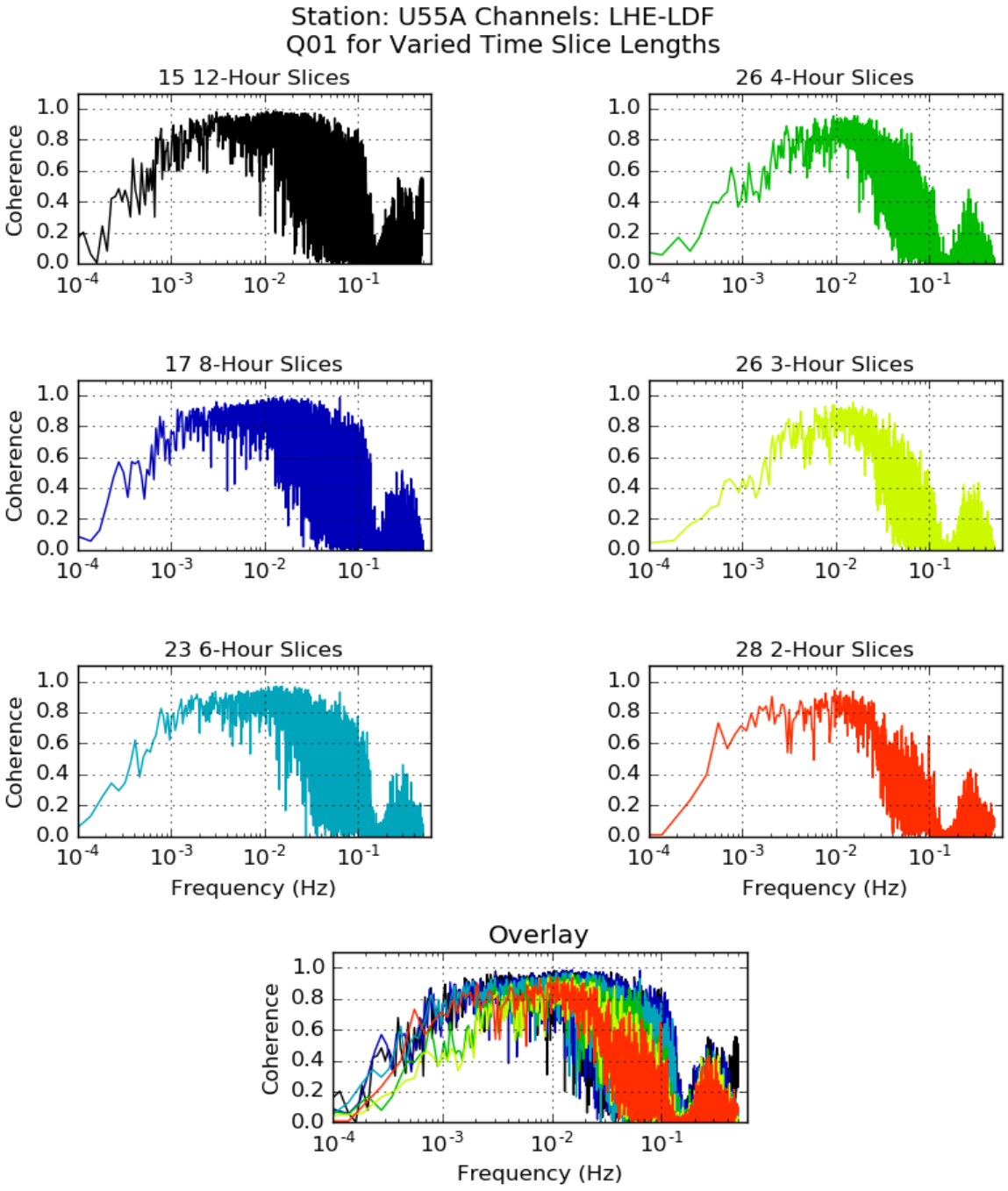

Figure 2-2. Comparison of coherograms for different length of record slices (i.e. varying the length of a Q)

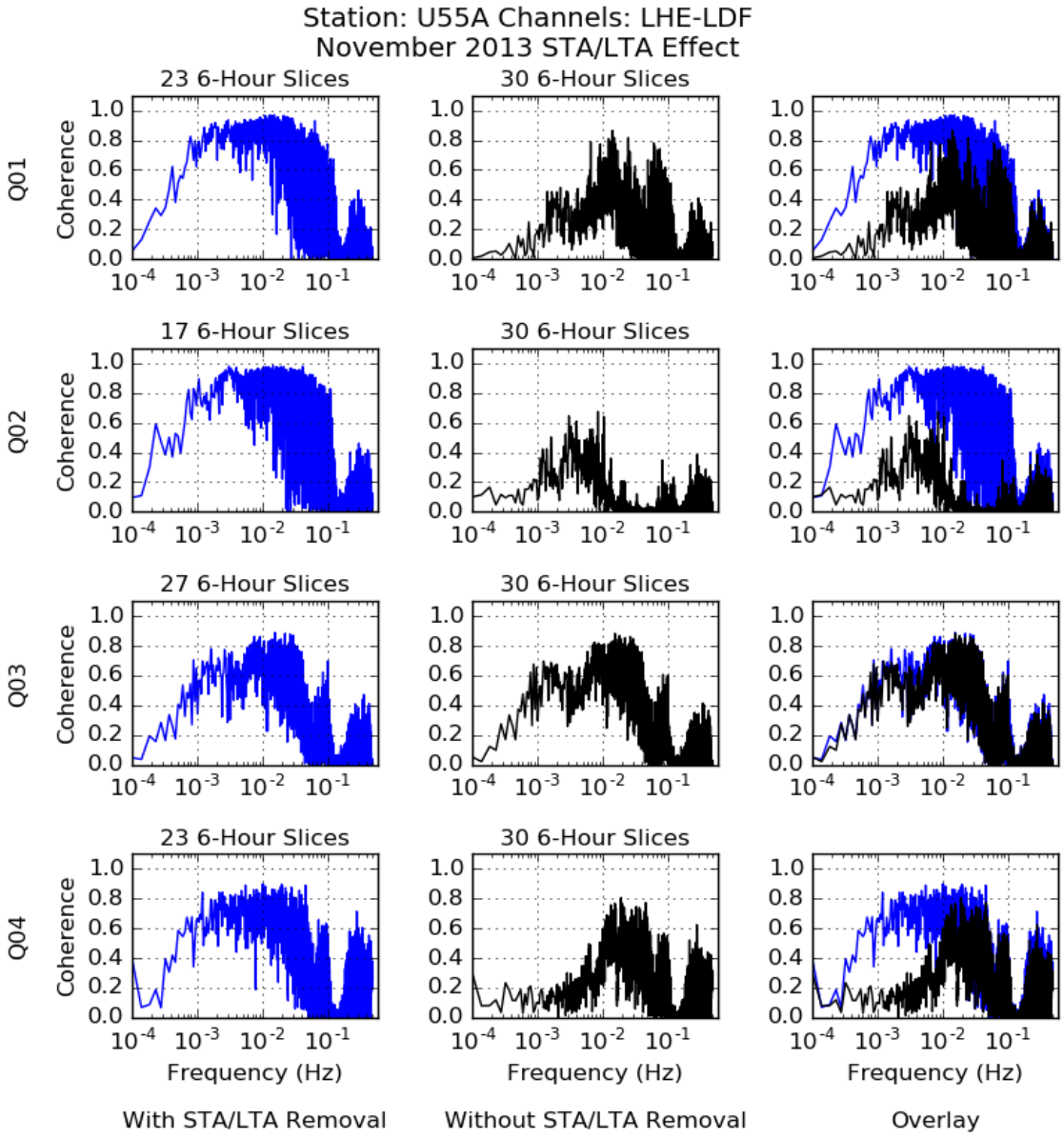

Figure 2-3. Comparison of coherograms showing effects of STA/LTA removal.

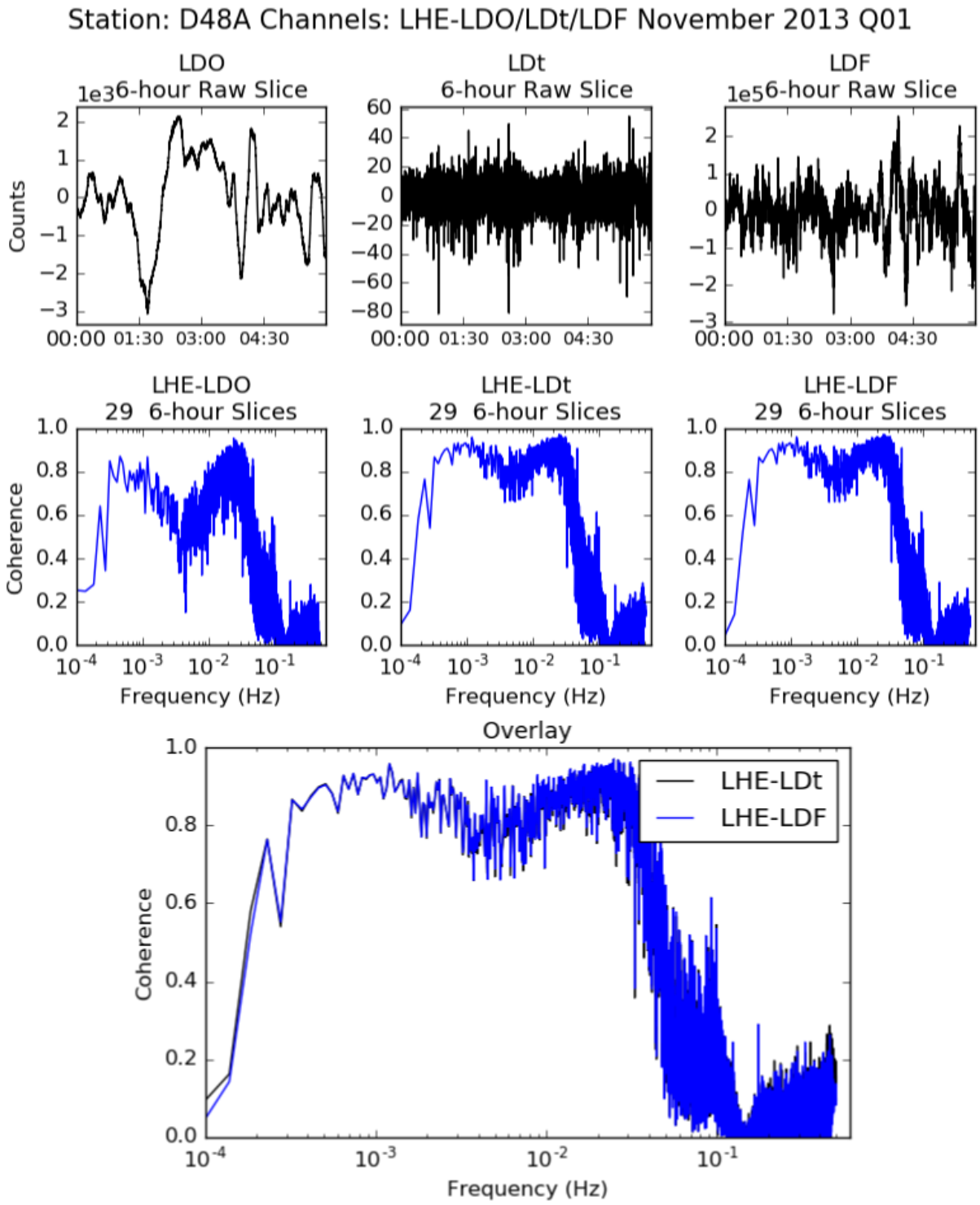

Figure 2-4. A comparison of coherograms for different atmospheric signals.

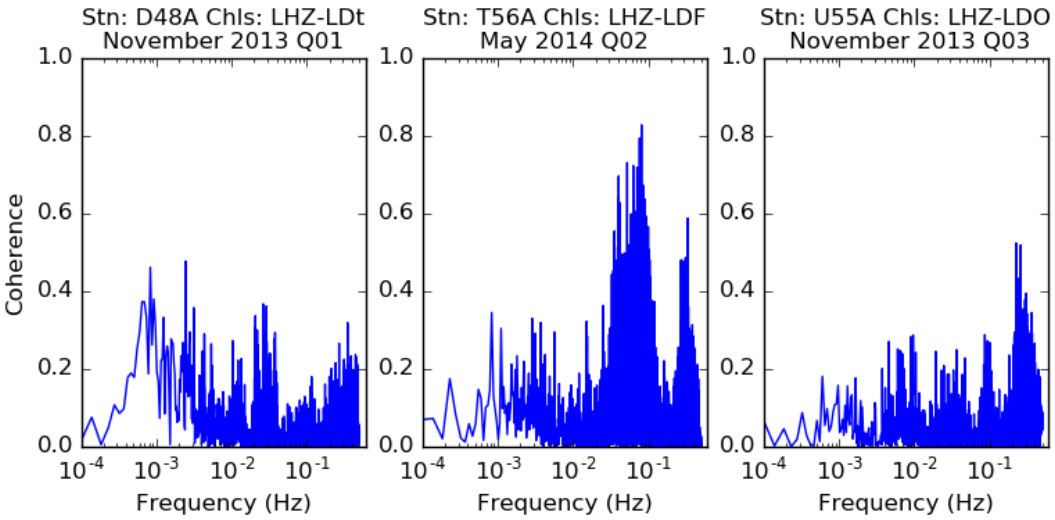

Figure 2-5. Three coherograms showing low coherence with vertical seismic channels.

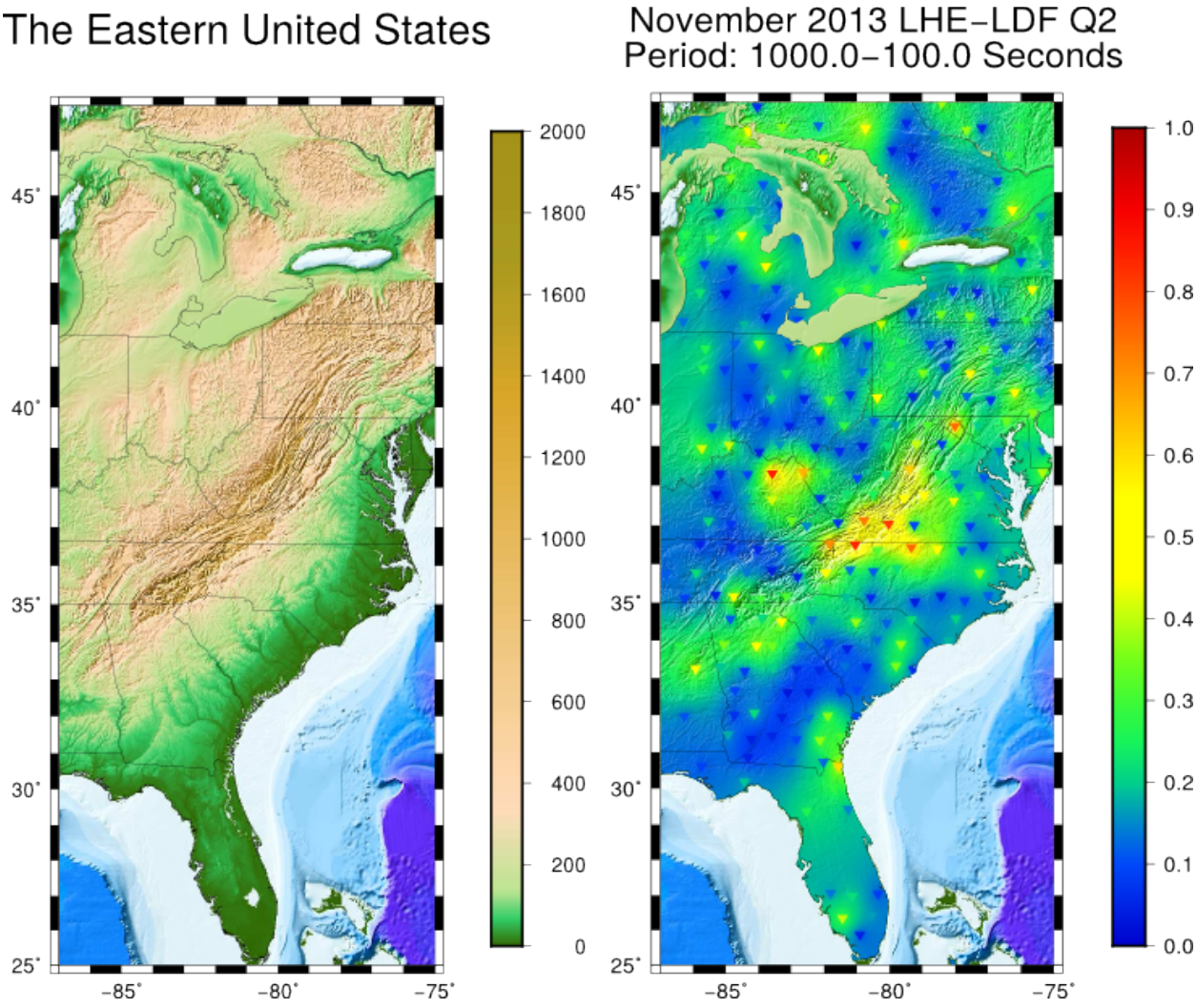

Figure 2-6. Digital Elevation Map (DEM) of study area (left) and same map overlain with interpolated coherence as calculated in November 2013 between channels LHE and LDF for the 1000-100 second period band.

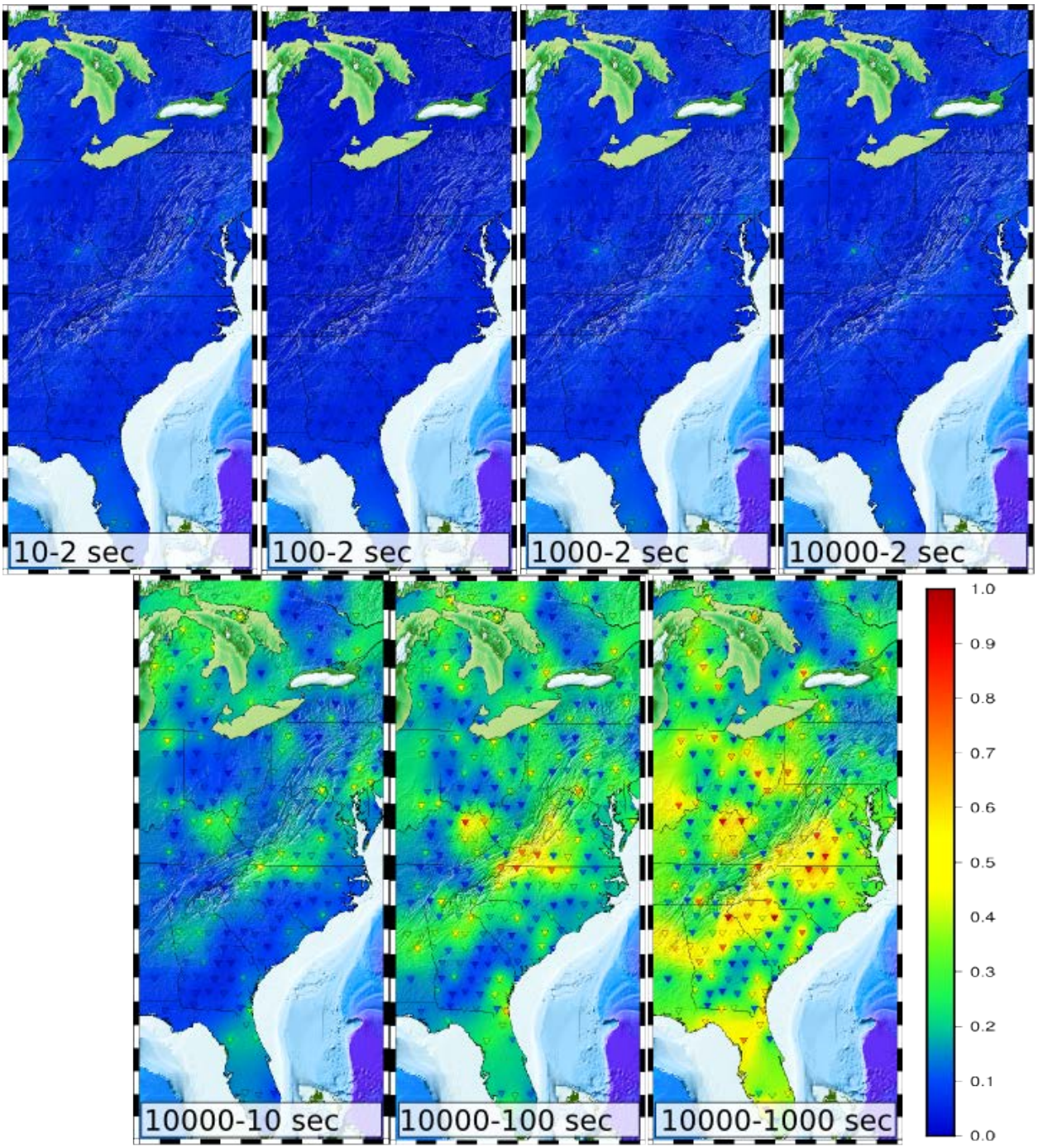

Figure 2-7. Coherence maps of varying period bands for November 2013, LHE seismic channel, and LDF infrasound channel.

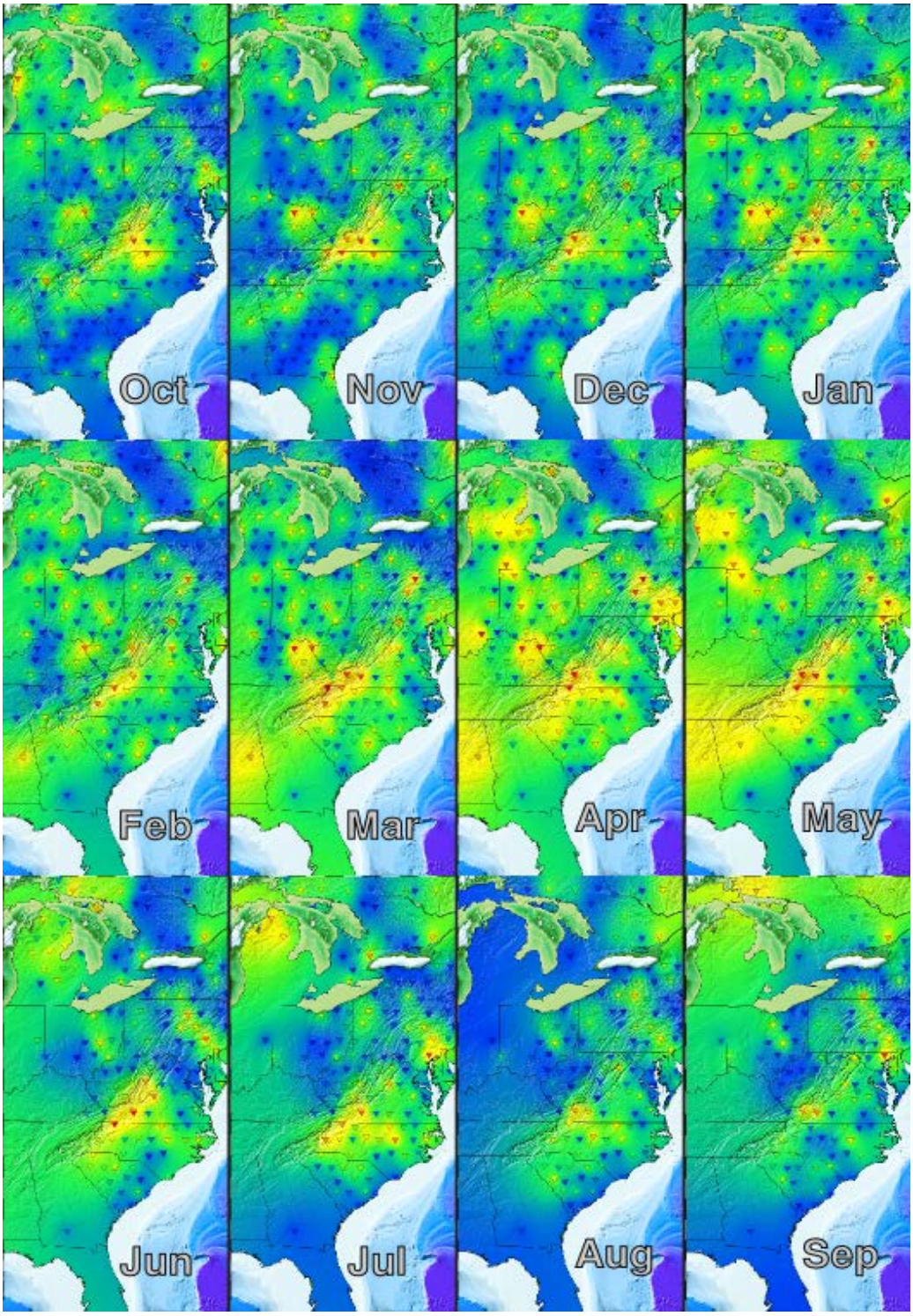

Figure 2-8. Coherence maps of LHE-LDF for 1000-100 s from October 2013 to September 2014.

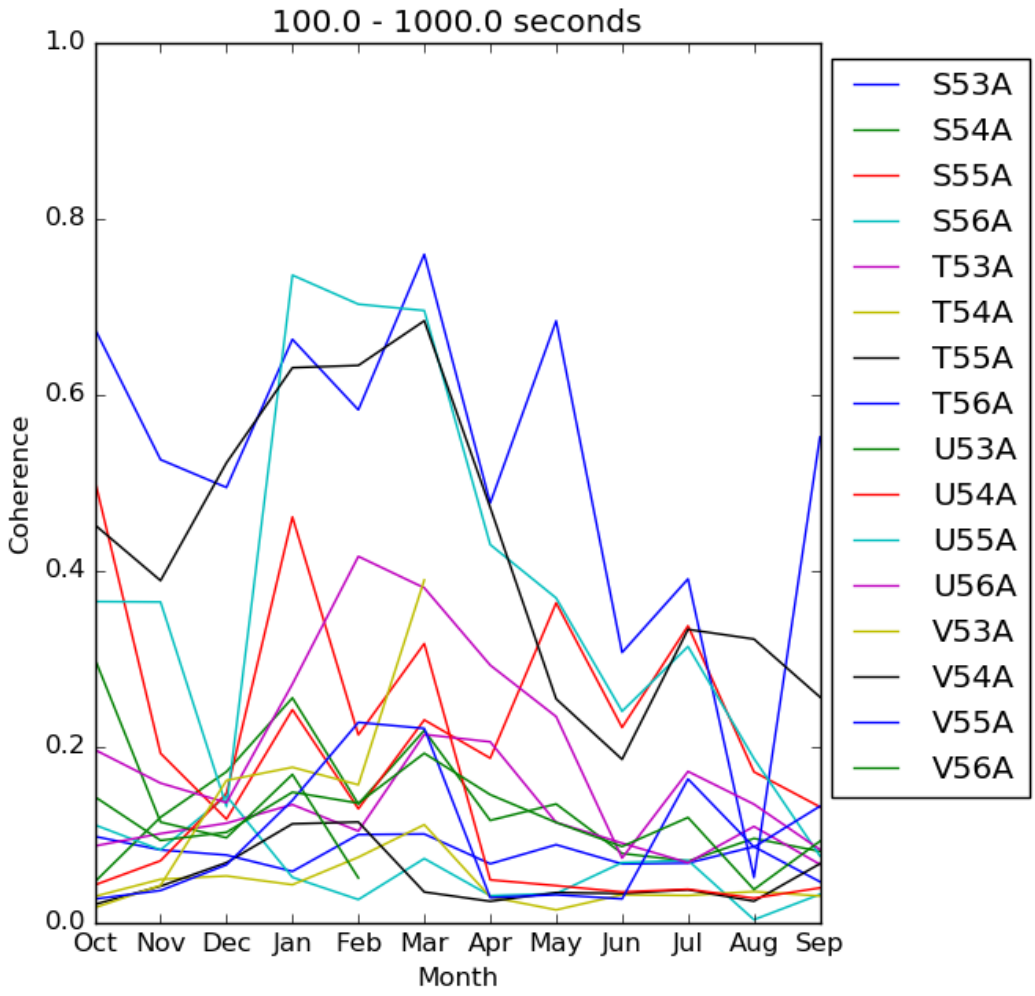

Figure 2-9. Monthly normalized coherence in the 1000-100 second period band for 16 stations.

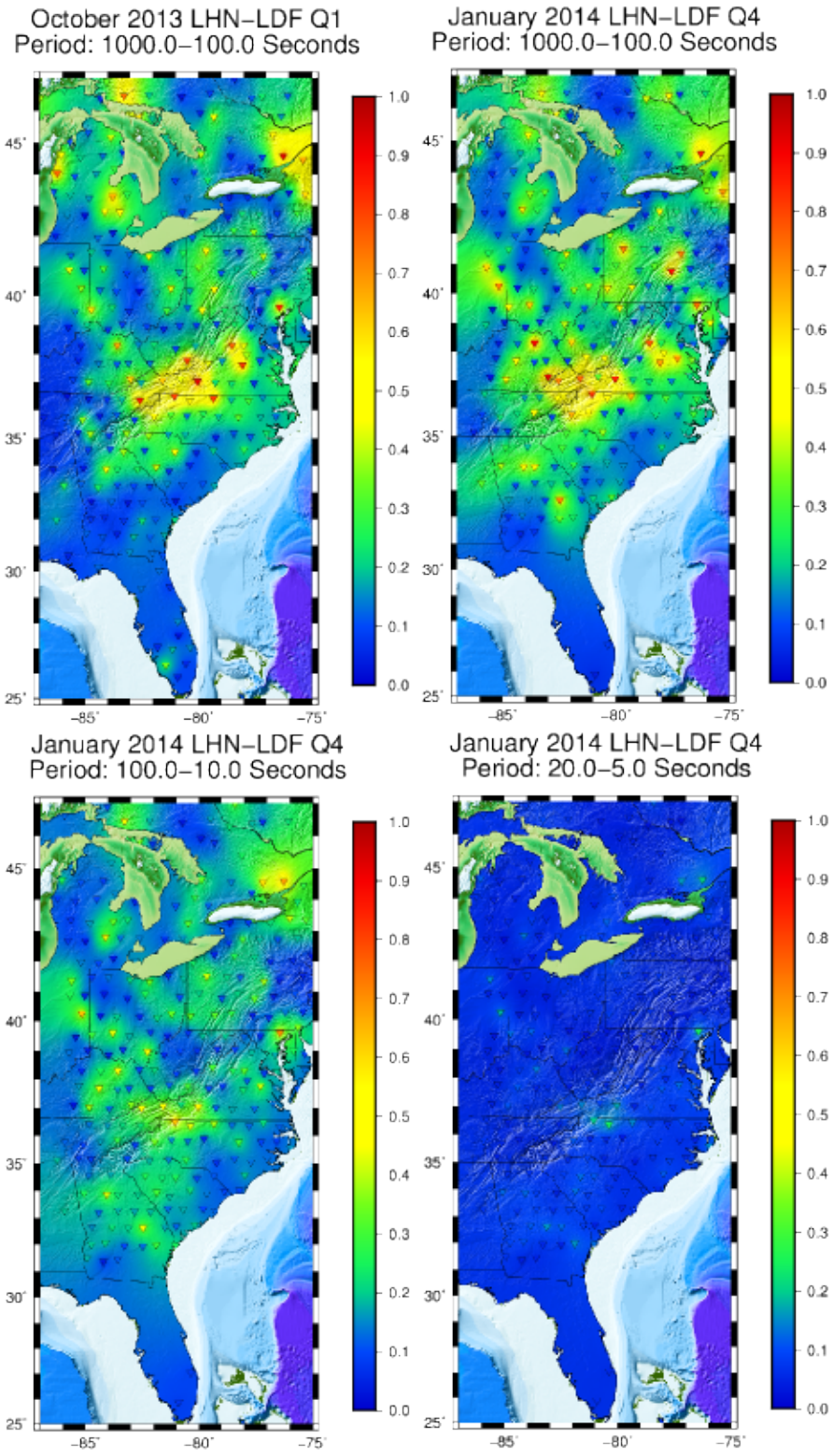

Figure 2-10. Assorted coherence maps for LHN-LDF

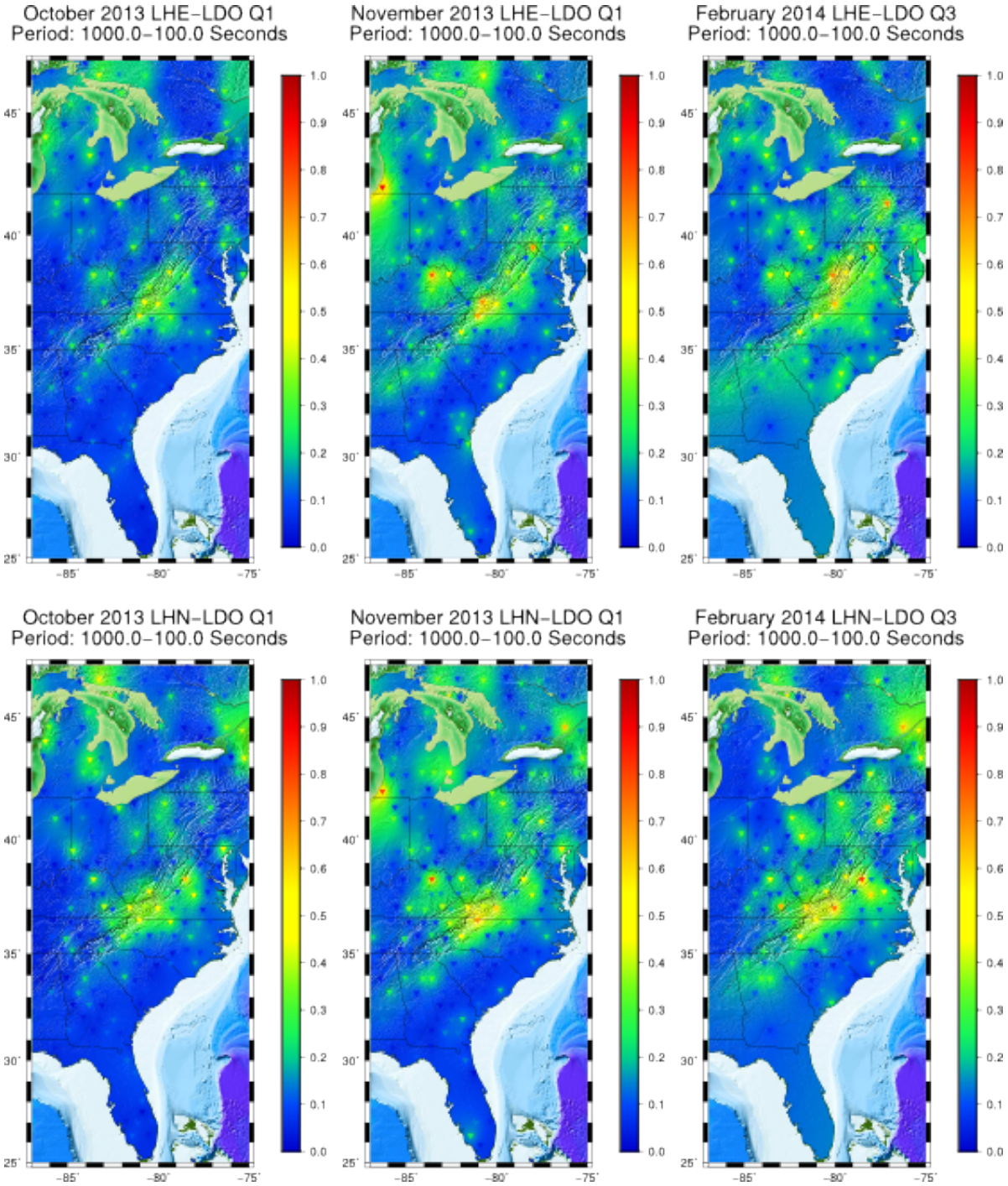

Figure 2-11. Coherence between horizontal seismic components and LDO shown for different months.

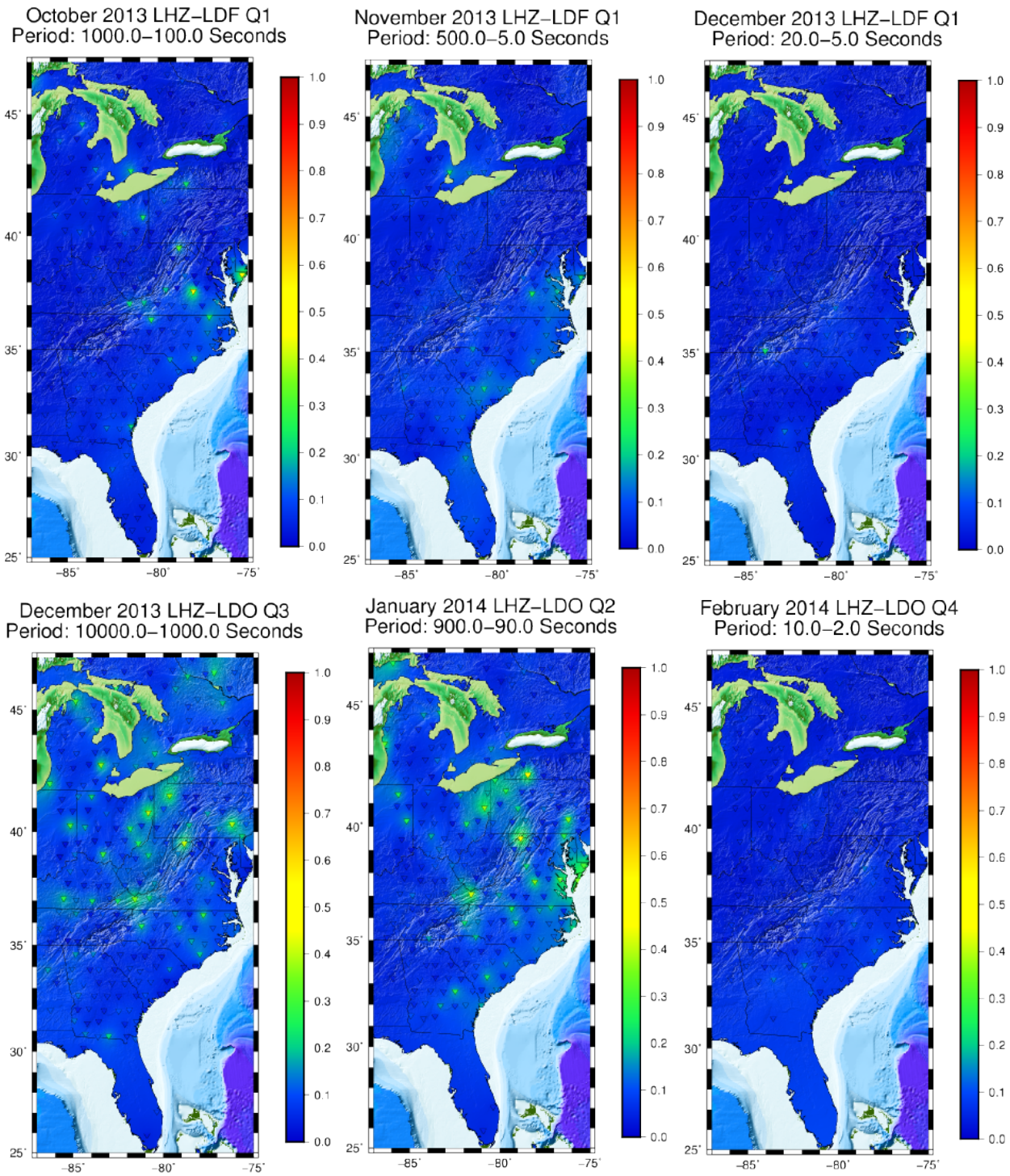

Figure 2-12. Coherence maps for LHZ-LDF and LHZ-LDO for varied months and frequency bands.

CHAPTER 3
DISCUSSIONS AND CONCLUSIONS

Our initial hypothesis was that topography would influence the coupling mechanism between atmospheric and seismic energy affecting how energy transfer from the atmosphere into the ground creates seismic noise. The two main components of topography are relief and slope. Our analyses do not evaluate the relative significance of each component; however, the highest coherence measurements are not measured at the stations with the highest elevation and therefore relief cannot be the sole factor in coupling efficacy. While our analyses do not identify a precise coupling mechanism, a correlation between heightened coherence and the Appalachian Mountain chain – a major topographic feature – is seen. This supported our initial hypothesis in at least three ways: location of high coherence stations, the channels that display high coherence, and relative time independence of coherence.

It is clear from many of the maps shown that the major groupings of heightened coherence align with the Appalachian mountain chain or are located at its bend. If the energy is transferring from the atmosphere into the ground this makes some intuitive sense as the mountain would provide resistance for a moving pressure signal in much the same way a speed bump would take energy away from a car speeding over it. If topography were irrelevant we would expect to see either no groupings of high coherence stations, or multiple significant groupings associated with other features.

Topography affecting atmosphere-ground coupling is further supported by high horizontal coherence and low vertical coherence. In the case where there was no significant coupling at all there would of course be low coherence across all three channels. One could also imagine a coupling mechanism in which energy was

transferred primarily by Newtonian attraction to air masses with varying densities or seismic energy reverberating outwards like a drum; however, in both of these cases there would be high coherence with the LHZ channel which is not observed in our data. The fact that we always see very low coherence when looking at the LHZ channel compared with heightened coherence for both horizontal channels supports the idea that noise from varying pressures is due to large scale tilting effects (e.g. Sorrells, 1971; De Angelis and Bodin, 2012).

Lastly, we see that coherence is not strongly dependent on time. There are some slight variations shown in time of day and monthly plots; however, there are no large seasonal effects observed nor strong diurnal patterns. This alone does not point to topography as a driver of coupling efficacy; however, it does allow us to rule out wind as a primary coupling mechanism because wind is known to have strong diurnal patterns.

Due to the intrinsic ambiguity in causal direction with coherence-based analyses, we cannot definitively characterize either pressure or infrasound as a seismic noise source. It is possible that seismic noise is coupled into the atmosphere, as has been demonstrated for large events (e.g. Yuen et al., 1969 and Weaver et al., 1970); however, this is not expected to be significant for the ambient seismic signals that we analyzed. It is also possible that there is no energy transfer, but rather that a third yet unidentified signal drives both signals at the high coherence locations – though the existence of an unidentified signal at this scale is unlikely. Figure 2-3 supports our hypothesized directionality by showing how coherence increases when STA/LTA methods remove data containing strong seismic signals (i.e. earthquakes). If energy

was primarily being transferred from the ground into the atmosphere than one would expect more energy to transfer during an earthquake and not lowered coherence.

While we can't ascertain the direction of energy transfer, it is clear that coupling between the atmosphere and the ground is stronger at long periods (> 100 seconds) than at shorter periods for the signals we analyzed. While this doesn't readily affect our hypothesis, it is relevant for any seismic research being done in this band, including normal mode analysis. If the energy is being transferred into the ground then these signals will act as noise obscuring normal mode signals and if the opposite is true than there is potential for the use of alternate data sets in finding normal modes. One way to test the direction of transfer would be to use deconvolution techniques to remove any atmospheric signal in the seismic record. Successful deconvolution of atmospheric noise would show clearer peaks at the known frequencies for normal modes, while attempting this deconvolution with an atmospheric signal that is seismically driven would result in a weakening of the hum signal. With the observed topographic coupling, we can identify stations likely to have improved long period signal recovery with the installation of either collocated barometric or infrasound arrays – and for this type of analysis we have shown that having both sensors is not necessary.

By analyzing one year of data from 419 seismic stations we have shown varied atmospheric coherence across the eastern half of the TA network. The most prominent cluster of high coherence stations is along the Appalachian mountain chain, which suggests a relationship between topography and atmosphere-ground coupling. When there is high coherence with pressure or infrasound signals and horizontal seismic signals it is in the long period band (>100 s) and the coherence information is equivalent

between the two atmospheric datasets if a time derivative of the pressure signal is used. We have shown that all stations have little to no atmospheric coherence in high frequency bands with horizontal channels, also in all frequency bands with vertical seismic signals.

Due to the low frequency band where coherence is observed, this work is most readily applicable to furthering research on normal modes. Depending on the directionality of the energy transfer, similar coherence analysis can be used to improve normal mode detection in seismic signals or possibly allow normal mode joint analysis with atmospheric and seismic signals. In either case, improved normal mode detection will advance our understanding of solid-earth structure and improved understanding of atmospheric noise coupling will improve site selection techniques for seismic installations. If atmosphere-ground coupling is better understood, it can also advance planetary seismology where remote sensing of the atmosphere and topography is significantly easier and cheaper to measure than it is to deploy seismometers, as suggested by for Venus by Garcia et al. (2005).

LIST OF REFERENCES

Anderson, D., Miller, W., Latham, G., Nakamura, Y., Toksoz, M., Daiynty, A., Duennebier, F., Lazarewicz, A., Kovach, R., and Knight, T. (1997) Seismology on Mars. *Journal of Geophysical Research*, 82, 4524-4546.

Ardhuin, F., Gualtieri, L., and Stutzmann, E. (2015) How ocean waves rock the Earth: Two mechanisms explain microseisms with periods 3 to 300 s. *Geophysical Research Letters*, 42, 765-772.

Beauduin, R., Lognonné, P., Montagner, J., Cacho, S., Karczewski, J., and Morand, M. (1996) The effects of the atmospheric pressure changes on seismic signals or how to improve the quality of a station. *Bulletin of the Seismological Society of America*, 86, 1760-1769.

Bertolini, A., Cella, G., DeSalvo, R., and Sannibale, V. (1999) Seismic noise filters, vertical resonance frequency reduction with geometric anti-springs: a feasibility study. *Nuclear Instruments and Methods in Physics Research*, 435, 475-483.

Bromirski, P.D., and Duennebier, F.K. (2002) The near-coastal microseism spectrum: Spatial and temporal wave climate relationship. *Journal of Geophysical Research*, 107, ESE 5-1 – ESE 5-20.

Cara, F., Di Giulio, G., and Rovelli, A. (2003) A study on the seismic noise variations at Colfiorito, central Italy: Implications for the use of H/V spectral ratios. *Geophysical Research Letters*, 30.

Cessaro, R.K. (1994) Sources of Primary and Secondary Microseisms. *Bulletin of the Seismological Society of America*, 84, 142 - 148.

De Angelis, S., and Bodin, P. (2012) Watching the wind: seismic data contamination at long periods due to atmospheric pressure-field-induced tilting. *Bulletin of the Seismological Society of America*, 102, 1255-1265.

Deuss, A., Irving, J.C.E., and Woodhouse, J.H. (2010) Regional Variation of Inner Core Anisotropy from Seismic Normal Mode Observations. *Science*, 328, 1018 - 1020.

Diaz, J., Villasenor, A., Morales, J., Pazos, A., Cordoba, D., Pulgar, J., Garcia-Lobon, J., Harnafi, M., C.R., Gallart, J., and the TopoIberia Seismic Working Group (2010) Background noise characteristics at the IberArray broadband seismic network. *Bulletin of the Seismological Society of America*, 100, 618-628.

Ekstrom, G. (2001) Time domain analysis of Earth's long-period background seismic radiation. *Journal of Geophysical Research*, 106, 26483-26493.

Forbriger, T. (2007) Reducing magnetic field induced noise in broad-band seismic recordings. *Geophys. J. Int.*, 169, 240-258.

Forbriger, T., Widmer-Schnidrig, R., Wielandt, E., H.M., and Ackerley, N. (2010) Magnetic field background variations can limit the resolution of seismic broad-band sensors. *Geophys. J. Int.*, 183, 303-312.

Garcia, R., Lognonné, P., and Bonnin, X. (2005) Detecting atmospheric perturbations produced by Venus quakes. *Geophysical Research Letters*, 32.

Hasselmann, K. (1963) Statistical analysis of the generation of microseisms. *Rev. Geophys.*, 1, 177-210.

Knapmeyer, M., Oberst, J., Hauber, E., Wahlisch, M., Deuchler, C., and Wagner, R. (2006) Working models for spatial distribution and level of Mars' seismicity. *Journal of Geophysical Research*, 111.

Kobayashi, N., and Nishida, K. (1998) Continuous excitation of planetary free oscillations by atmospheric disturbances. *Nature*, 295, 357-360.

Kurrle, D., and Widmer-Schnidrig, R. (2008) The horizontal hum of the Earth: A global background of spheroidal and toroidal modes. *Geophysical Research Letters*, 35.

Longuet-Higgins, M. (1950) A Theory of the Origin of Microseisms. *Philos. Trans. Roy. Soc.*, 243, 1-35.

McNamara, D., and Buland, R. (2004) Ambient noise levels in the continental United States. *Bulletin of the Seismological Society of America*, 94, 1517-1527.

Merriam, J. (1992) Atmospheric pressure and gravity. *Geophys. J. Int*, 109, 488-500.

Nishida, K., Kobayashi, N., and Fukao, Y. (2002) Origin of Earth's ground noise from 2 to 20 mHz. *Geophysical Research Letters*, 29, 52-1 – 52-4.

Panning, M., Beucler, E., Drilleau, M., Mocquet, A., Lognonné, P., and Banerdt, B. (2015) Verifying single-station seismic approaches using Earth-based data: Preparation for data return from the InSight mission to Mars. *Icarus*, 248, 230-242.

Peterson, J. (1993) Observations and Modelling of Seismic Background Noise. *USGS Open File Report 93-322*.

Rhie, J., and Romanowicz, B. (2004) Excitation of Earth's continuous free oscillations by atmosphere-ocean-seafloor coupling. *Nature*, 431, 552-556.

Rodgers, P., Taylor, S., and Nakanishi, K. (1987) System and site noise in the regional seismic test network from 0.1 to 20 Hz. *Bulletin of the Seismological Society of America*, 77, 663-678.

Schimmel, M., and Paulssen, H. (1997) Noise reduction and detection of weak, coherent signals through phase-weighted stacks. *Geophys. J. Int.*, 130, 497-505.

Sorrells, G. (1971) A Preliminary Investigation into the Relationship between Long-Period Seismic Noise and Local Fluctuations in the Atmospheric Pressure Field. *Geophys. J. R. astr. Soc.*, 26, 71-82.

Stehly, L., Campillo, M., and Shapiro, N. (2006) A study of seismic noise from its long range correlation properties. *Journal of Geophysical Research*, 111.

Suda, N., Nawa, K., and Fukao, Y. (1998a) Earth's background free oscillations. *Science*, 279, 2089-2091.

Suda, N., Nawa, K., and Fukao, Y. (1998b) Earth's Background Free Oscillations. *Science*, 279, 2089-2091.

Tanimoto, T. (2008) Geophysics: Humming a different tune. *Nature*, 452, 539-541.

Tanimoto, T., and Um, J. (1999) Cause of continuous oscillations of the Earth. *Journal of Geophysical Research*, 104, 28723-28739.

Warburton, R., and Goodkind, J. (1977) The influence of barometric pressure variations on gravity. *Geophys. J. R. astr. Soc.*, 48, 281-292.

Weaver, P.F., Yuen, P.C., and Prolss, G.W., F.A.S. (1970) Acoustic coupling into the ionosphere from seismic waves of the earthquake at Kurile Islands on August 11, 1969. *Nature*, 226, 1239-1241.

Wilson, D., Leon, J., Aster, R., Ni, J., Schlue, J., Grand, S., Semken, S., Baldridge, S., and Gao, W. (2002) Broadband seismic background noise at temporary seismic stations observed on a regional scale in the southwestern United States. *Bulletin of the Seismological Society of America*, 92, 3335-3342.

Withers, M., Aster, C., Young, C., and Chael, E. (1996) High-frequency analysis of seismic background noise as a function of wind speed and shallow depth. *Bulletin of the Seismological Society of America*, 86, 1507-1515.

Yuen, P.C., Weaver, P.F., Suzuki, R.K., and Furumoto, A.S. (1969) Continuous, traveling coupling between seismic waves and the ionosphere evident in May 1968 Japan earthquake data. *Journal of Geophysical Research*, 74, 2256-2264.

Zurn, W., and Widmer, R. (1995) On noise reduction in vertical seismic records below 2 mHz using local barometric pressure. *Geophysical Research letters*, 22, 3537-3540.

BIOGRAPHICAL SKETCH

Matt Farrell grew up in Rotterdam, New York and graduated Mohonasen High School in 2008. He has always been curious and constantly questioning. This passion for learning paired with a passion for teaching led him to study physics and secondary education at SUNY Geneseo. Along the way a favorite professor defined geophysics as “using the tools and methods of physics to answer the questions of geology.” This hooked Matt and he graduated with a BA in geophysics in 2012. In 2013 Matt began studying seismology at the University of Florida using Python to understand connections between the atmosphere and the solid-earth. While he enjoyed various aspects of the research, teaching over 10 semesters of physics and geology students between both universities affirmed his passion for teaching and he is now eager to pursue a career in education.